Optica Applicata, Vol. LV, No. 2, 2025
DOI: 10.37190/oa/203754

Based on multi-layer gradient threshold CFRP plates defects detection system

YUXIANG FENG[1,*], XIANG JU[2], WENJING GUO[3]

[1]College of Intelligent Manufacturing Engineering, Shanxi Institute of Science and Technology, Jincheng 048000, Shanxi, China

[2]Department of Automation, Taiyuan Institute of Technology, Taiyuan 030008, Shanxi, China

[3]Department of Electronic Engineering, Taiyuan Institute of Technology, Taiyuan 030008, Shanxi, China

[*]Corresponding author: fengyuxiang0112@sina.com

Carbon fiber reinforced plastic (CFRP) is widely used in fields such as aircraft and construction due to its advantages of light weight, high hardness, wear and corrosion resistance. To quantitatively detect internal defects in CFRP panels, a THz reflective defect detection system was built. A defect analysis algorithm based on multi-layer gradient threshold is proposed. Based on the manufacturing process of CFRP, a THz wave echo function model for multi-layer CFRP structures was derived. A CFRP plate containing debonding defects and crack defects was trial produced, to obtain its THz time-domain spectrum. The experiment completed the reconstruction of THz two -dimensional images of CFRP plates. The test results show that three different depths of test data can be detected, and the calculated diameters of the debonding defect areas are 9.12, 9.86, and 9.93 mm, respectively, with a relative error mean of 3.63%. Crack defects can also be effectively identified, but the quality of their test images will decrease with increasing pre-embedded depth. The linearity between defect depth and testing frequency is 0.98, which verifies the possibility of quantitative calculation. The test results of power spectral density and defect depth show that it has good uniformity.

Keywords: defects detection, THz spectrum, multi-layer gradient threshold algorithm, carbon fiber reinforced plastic (CFRP).

1. Introduction

Composite materials are composed of different materials mixed in different proportions, among which CFRP are widely used in aerospace, construction, medical and other fields due to their advantages of high temperature resistance, corrosion resistance, and light weight [1]. However, defects such as voids, inclusions, and cracks may occur during its manufacturing process. How to accurately identify defects without damaging its structure has become a research hotspot.

Common non-destructive testing methods [2] include ultrasonic testing, infrared testing, X-ray testing, and THz testing. Although ultrasonic testing does not require damage to the structure of the test object, it requires contact with the test object and the use of coupling agents to enhance the echo signal. And the spatial resolution of ultrasound is low, making it unsuitable for crack detection. Infrared detection method can achieve non-contact rapid recognition, but its spatial resolution is limited. The X-ray detection method has high spatial resolution and can be used for identifying various types of defects, but X-rays are harmful to the human body, greatly limiting their application scenarios. In contrast, THz non-destructive testing technology [3, 4] has good penetrability to non-metallic materials and is harmless to the human body, making it an important means of defect detection for CFRP.

ZANDONELLA [5] uses THz wave band to conduct nondestructive testing on aviation foam materials, and its depth resolution is 0.5 mm. WANG *et al.* [6,7] used THz for quantitative detection of explosives, the concentration detection accuracy of the system is better than 0.50 mg/m^3, with an error of less than 5%. DESTIC *et al.* [8] qualitatively identified delamination defects using a THz light source and obtained test results showing the sensitivity of delamination defect location to laser polarization direction. REN *et al*. [9-11] used terahertz time-domain spectroscopy to study high-temperature resistant ceramic matrix composites (CMC), which can obtain defect size and depth information through time difference. This is of great significance for defect detection in aviation materials, with a defect position error of less than 0.5 mm. In 2020, they tested 500 μm debonding defects using image fusion algorithms, with an error of better than 6.8%. In 2021, they proposed a THz feature enhancement method based on continuous wavelet transform, which achieved a layered defect recognition accuracy of 0.3 mm in 6 mm thick GFRP. JIE *et al*. [12] constructed a multi-layer thickness simultaneous measurement method based on the Rouard model using THz time-domain signals, with an accuracy of approximately 0.5 mm. ZHEN *et al*. [13] conducted defect detection on highly integrated packaged chips, which can identify defect areas with an accuracy of 0.24 mm.

In summary, the THz detection method has been applied to detect various types of defects in various materials. However, most literature focuses on identifying a specific type of defect, and there are few reports on quantitatively identifying multiple types of defects simultaneously. This paper mainly focuses on the problem of simultaneous quantitative identification of defects of different depths and types. Starting from the detection mechanism of different defect types, this article improves the scanning structure of traditional THz non-destructive testing systems and proposes a multi-layer gradient threshold algorithm for rapid quantitative identification of multiple defect types.

2. System design

The system uses femtosecond laser to provide optical excitation, and the beam splitter divides the incident light into two beams. A beam is modulated by a time delay control

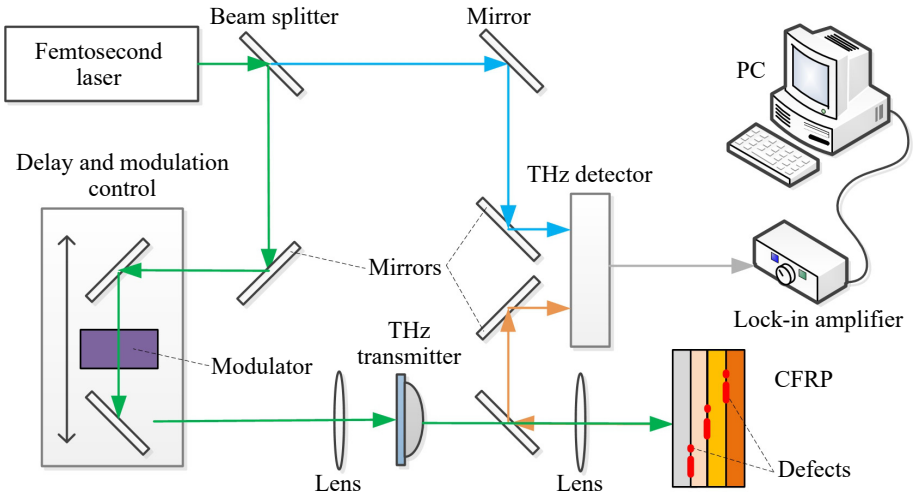

Fig. 1. Reflective THz detection system for CFRP.

unit and finally irradiated onto a CFRP board through a THz emitter. The THz wave reflected by the target is received by the THz detector together with another wave, and finally collected by the lock-in amplifier and imported into the computer. The overall structure of the system is shown in Fig. 1. This system achieves defect detection by analyzing multiple echo signals generated by irradiation on CFRP plates. The system analyzes terahertz time-domain spectroscopy (THz TDS) [14] to obtain depth and breadth information of internal defects in CFRP.

The THz source is generated by laser pulses generated by a mode-locked titanium sapphire femtosecond laser. The pump pulse passes through a chopper with a frequency of 1.1 kHz and enters the photoconductive antenna to excite THz waves. THz waves are collimated and focused on a CFRP plate, and then focused and collimated on a THz receiver through an off-axis parabolic mirror. This signal and the signal emitted by the source are controlled by a computer to achieve controllable optical path difference, thus completing signal sampling. The THz TDS system has a spectral range of 0.3 to 2.4 THz, a spectral resolution of 2.9 GHz, and a signal-to-noise ratio (SNR) better than 68.0 dB. The detection end has a two-dimensional scanning platform that can complete scanning imaging within a range of 10 cm to 10 cm in the x and y directions of the test area.

3. Multi-layer gradient threshold detection model

Due to the repeated stacking of CFRP, its structure can be seen as a multi-layer combination. The emitted laser is placed vertically with the CFRP plate. When irradiating CFRP plates, most of the reflected signals have a certain angle when they are emitted, except for the vertical incident position. The angle is θ. The expression of this angle is used to calculate more general situations. Along the z-axis, if the first interface position is $z = 0$ and the last exit interface position is $z = z_i$, then the electromagnetic

wave matrix can be represented as M_1, M_2, …, M_i. The electric field propagating forward along the z-axis in the structure is E^+, and the electric field propagating backward is E^-, and $E = E^+ + E^-$ [15]. Among them, the magnetic permeability and dielectric constant of each layer are μ_i and ε_i, respectively. When THz waves propagate in a layered structure, reflection waves are generated at each level of the interface due to interface reflection, as shown in Fig. 2. The setting of multi-layer gradient threshold is determined based on the accuracy of the number of layers and defect recognition depth of the test target. Because the echo signal intensity reflected by interfaces at different depths varies, as long as the intensity signal extraction is completed for the defect free and defect free states at that depth, the test results of the two states can be used as the threshold upper and lower limits. Then, the thresholds of different layers will also change accordingly, and they can all be obtained through measurement. The functional relationship between imaging frequency and defect depth will be presented in the experiment.

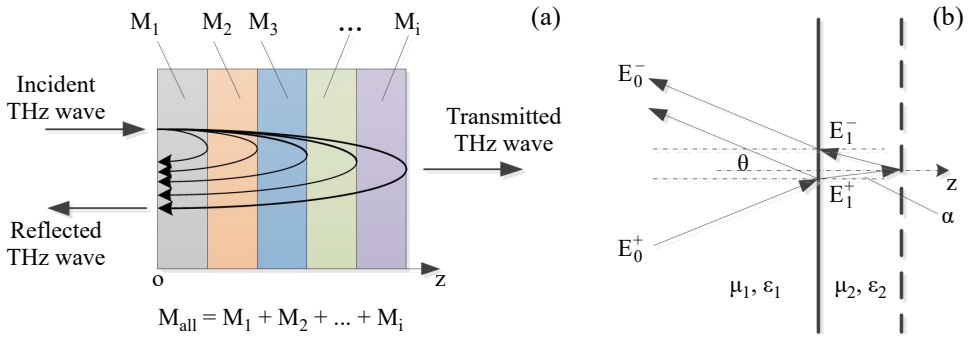

Fig. 2. Propagation of THz waves in multi-layer composite materials. (a) Layered structure of composite materials. (b) Electric vector path on layered interface.

From Fig. 2, it can be seen that the system adopts a time-domain analysis method, so as long as it is not in the same echo period, it will not affect the signal of the corresponding test surface. So the roughness of the surface has almost no effect on the testing. Electromagnetic waves can be divided into vertical and parallel components, with the vertical component being the tangential component [16]. For multiple reflections, the electric field can be expressed as

$$\begin{cases} E_1^+\big|_\perp = t_{01}E_0^+\big|_\perp + r_{10}E_1^-\big|_{||} \\ E_0^-\big|_{||} = r_{01}E_0^+\big|_\perp + t_{10}E_1^-\big|_{||} \end{cases} \tag{1}$$

Among them, $E^+\big|_\perp$ represents the vertical component of E^+, and $E^+\big|_\perp = E^+\cos\theta$. $E^-\big|_\perp$ represents the horizontal component of E^-, $E^-\big|_{||} = E^-\cos\theta$. t_{ij} and r_{ij} are the transmission and reflection coefficients from medium i to medium j, and n_i is the com-

plex refractive index of the material. For TE waves, the transmission coefficient and reflection coefficient have

$$\begin{cases} r_{01} = \dfrac{n_0\cos\theta - n_1\cos\alpha}{n_0\cos\theta + n_1\cos\alpha} \\ t_{01} = \dfrac{2n_0\cos\theta}{n_0\cos\theta + n_1\cos\alpha} \end{cases} \tag{2}$$

The electric vector matrices on both sides can be represented as

$$\begin{bmatrix} E_0^+\big|_\perp \\ E_0^-\big|_{||} \end{bmatrix} = \frac{1}{t_{01}} \begin{bmatrix} 1 & r_{10} \\ r_{01} & 1 \end{bmatrix} \begin{bmatrix} E_1^+\big|_\perp \\ E_1^-\big|_{||} \end{bmatrix} \tag{3}$$

According to the time harmonic effect, there exists a phase matrix P_n on both sides of the medium, which can be expressed as

$$P_n = \begin{bmatrix} \exp(-i\delta_n) & 0 \\ 0 & \exp(i\delta_n) \end{bmatrix}, \quad \delta_n = 2\pi k_0 \sqrt{\frac{\varepsilon_n}{\mu_n}}\, d_n \cos\varphi_n \tag{4}$$

Among them, carbon fiber material is a non-polar material, with $\mu = 1$, $\varepsilon/\mu = n^2$, and d_n is the thickness of the n-th layer of the medium; φ_n is the angle of retransmission. And its amplitude matrix I can be expressed as

$$I_{i,\,i+1} = \frac{1}{t_{i,\,i+1}} \begin{bmatrix} 1 & r_{i,\,i+1} \\ r_{i,\,i+1} & 1 \end{bmatrix} \tag{5}$$

When extending Eqs. (4) and (5) from the first layer to the n-th layer, Eq. (3) yields

$$\begin{bmatrix} E_0^+\big|_\perp \\ E_0^-\big|_{||} \end{bmatrix} = I_{01}P_1I_{12}P_2\ldots P_NI_{N(N+1)} \begin{bmatrix} E_{N+1}^+\big|_\perp \\ E_{N+1}^-\big|_{||} \end{bmatrix} \tag{6}$$

To achieve the optimal value of multi-layer gradient threshold, the transfer function of THz waves at each layer interface is integrated. Thus, if M is defined as the transfer function of the entire multi-layer structure, then there is

$$M = I_{01}P_1I_{12}P_2\ldots P_NI_{N(N+1)} \tag{7}$$

Among them, the transmission coefficient and reflection coefficient of the layered structure are

$$r = \frac{E_0^-\big|_{\parallel}}{E_0^+\big|_{\perp}}, \qquad t = \frac{E_{N+1}^+\big|_{\perp}}{E_0^+\big|_{\perp}} \tag{8}$$

This result indicates that the transmission and reflection coefficients of the corresponding layer can be calculated based on the light intensity. Meanwhile, the time-domain spectrum of THz can be used to calculate the echo intensity at the corresponding position based on the echo time of the signal. Therefore, by converting the measured light intensity value into electric field intensity and inputting it into Eq. (8), the transmission coefficient and reflection coefficient at that position can be obtained. Based on the magnitude of the coefficient, it is possible to analyze whether there is debonding at that location.

4. Design and testing of CFRP test piece

4.1. CFRP test pieces with defects design

The size of the CFRP test piece is 50 to 100 mm, with a thickness of 20 mm. Its laying method is [0°/60°/–60°]. In order to quantitatively analyze the internal defects of CFRP through THz spectroscopy, two types of defects, circular debonding and cracks, were pre-embedded during the processing of CFRP. Each type of defect is pre-embedded at 3 depths for testing, at positions 5, 10, and 15 mm from the surface. Using a 10 mm diameter and 0.2 mm thickness polytetrafluoroethylene (PTFE) sheet to simulate circular hole debonding defects. The adhesive used for pasting is CD2018 epoxy resin adhesive produced by SIRNICE company. Because adhesive has strong fluidity

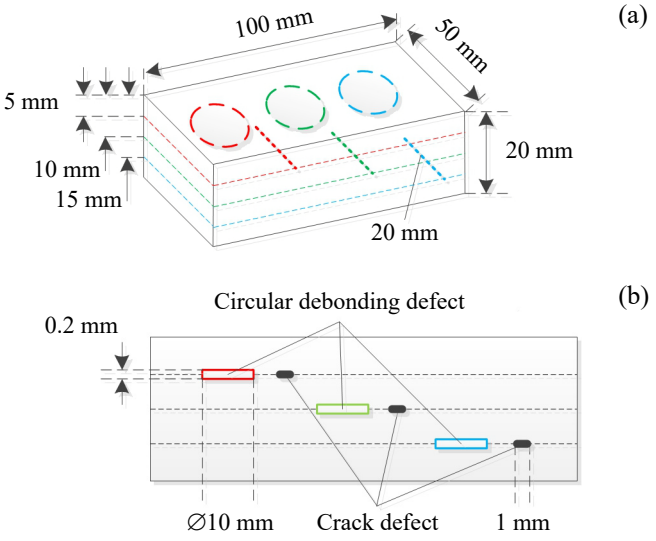

Fig. 3. CFRP test piece and defect structure design. (a) CFRP test piece 3D structure. (b) Defect size and location.

before curing, leaving gaps can easily cause reflux. Therefore, using PTFE sheets to simulate circular hole debonding defects can ensure the accuracy of defect area detection. A metal wire with a length of 20 mm, width of 1 mm, and depth of 0.2 mm is used to simulate crack defects by pulling it away from the edge of CFRP after forming. The structural form is shown in Fig. 3.

4.2. Comparison of time-domain test signals

The system conducts comparative testing on the locations of CFRP test pieces with no defects and those with debonding defects. By using Fourier transform to obtain the spectral information of THz echo, there will be a reflected wave at each interface position in the time-domain signal. If there is a defect in the CFRP module, a defect depth of 0.2 mm will result in a clear reflection peak in the time-domain signal. Meanwhile, the corresponding frequency domain values of these time-domain signals can also be extracted after Fourier transform, thus completing the inversion of defect depth. The THz time-domain signals with and without defects are shown in Fig. 4.

As shown in Fig. 4(a), the black line represents the response curve of THz echo without defects, and the red line represents the response curve of THz echo with defects. When the testing time is between 30 and 50 ps and there are no debonding defects at the corresponding testing depth position, the amplitude of the echo light does not fluctuate significantly, with a maximum value of 44.32 and a minimum value of –28.47. When there is a debonding defect, the maximum optical amplitude is 151.23 and the minimum is –148.95. The time difference between peak values is 1.56 ps, and the thickness of the debonding defect is 0.194 mm, with a relative error of 3.2%. As shown in Fig. 4(b), when there are no crack defects between 30 and 50 ps, the amplitude of the reflected light does not change significantly. There is not much fluctuation, with a maximum value of 27.92 and a minimum value of –35.64. When there is a crack defect, the maximum optical amplitude is 61.22 and the minimum is –73.54. The time differ-

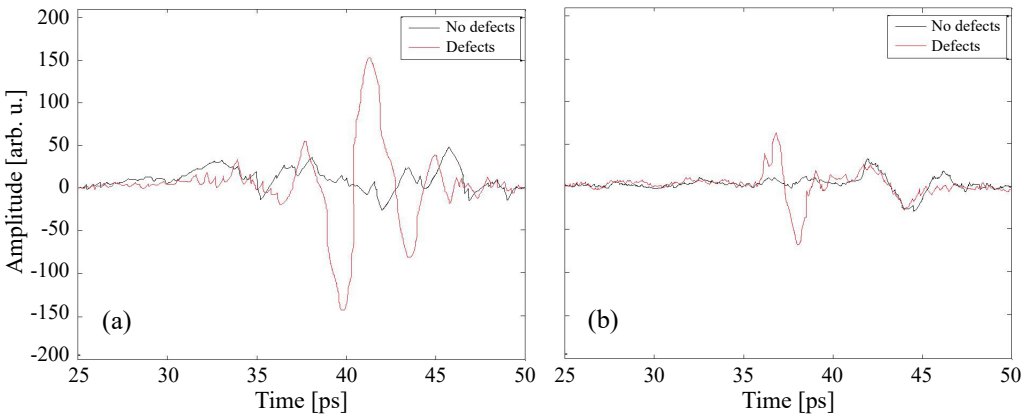

Fig. 4. Comparison of THz time-domain echo curves with and without defects. (a) Degumming defect, and (b) crack defect.

ence between peak values is 1.36 ps, and the thickness of the debonding defect is 0.169 mm, with a relative error of 15.5%. It can be seen that the system has a high recognition rate for debonding defects with small errors. It can also effectively identify crack defects, but the error is relatively large.

5. Experiments

5.1. THz image reconstruction

The THz source was used to scan and image the CFRP test sample, the distance from the THz source to the surface of the CFRP plate is 30 cm ± 2 cm, and the results are shown in Fig. 5.

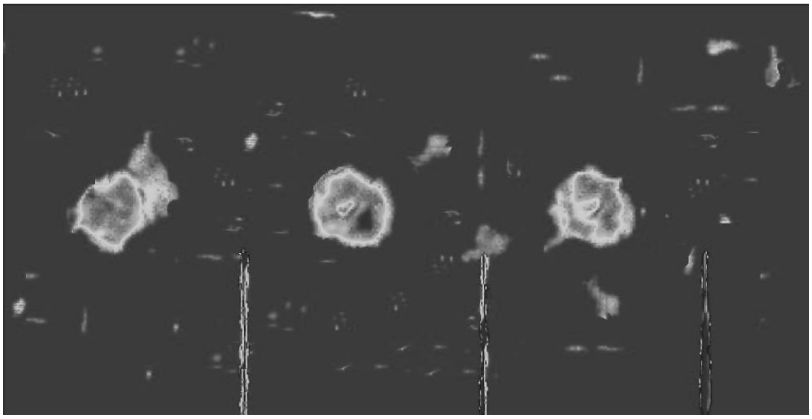

Fig. 5. Stress field distribution of trains under different load conditions.

As shown in Fig. 5, the images of three debonding defects are very obvious. On the right side of the first debonding circular hole defect, there is a protruding part with an irregular shape. This may be due to the presence of air during the placement of the PTFE sheet, and the failure to release air during the installation of CFRP resulted in the formation of an excess debonding layer in its vicinity. And this also indicates that if there is an air gap, two-dimensional THz images can be effectively recognized. The shapes of the other two debonding defects are relatively intact. The diameters of the circles corresponding to the three areas of debonding defects are 9.12, 9.86, and 9.93 mm, respectively. Their average relative error is 3.63%. And the testing results of debonding defects at different depths are relatively clear, with high detection rate. In contrast, the detection rate of cracks is slightly lower. The first two of the three cracks in the picture are more obvious, which are 5 and 10 mm, respectively. And the clarity of the 15 mm deep crack effect crosses. Although cracks can also be seen, their edge effect is weak. Some of these small noises are impurity noise, while others are noise caused by uneven density of carbon fibers. However, due to its small size, it has no impact on the structural strength.

5.2. Defect identification

The identification of defects includes defect type, defect depth, and defect size. For the type of defect, it can be determined by the shape of the defect in the THz image. Usually, debonding and interlayer defects will result in a substantial echo peak, which appears as a white area on the image, and the higher the brightness of the white area, the thicker the defect. The defects of crack types mainly rely on edge judgment. The determination of defect type belongs to qualitative judgment, while defect depth and size are quantitative judgments.

For the depth of defects, the judgment is based on the time signal of THz echo. The relationship between test depth and test frequency can be obtained by Fourier transform of the echo signal, thereby calculating the depth information of defects. The functional relationship between imaging frequency and defect depth is shown in Fig. 6(a). At the same time, in order to ensure a certain signal-to-noise ratio of the echo signal, appropriate power needs to be used at different depths. The test curves of frequency and power spectra in the range from 0.3 to 2.4 THz are shown in Fig. 6(b).

The relationship between defect depth and testing frequency is shown in Fig. 6(a). The system is based on time-domain testing, and there is a functional relationship between the testing depth and imaging frequency. The linear test curve indicates that the testing system can calculate the current testing depth based on changes in testing frequency. With the increase of defect depth, the frequency and defect depth show a linear upward trend. Analysis suggests that the absorption rate of the debonding defect layer is much lower than that of CFRP, so the closer it is to the test surface, its reflected echo signal will be stronger. Meanwhile, as the depth of the defect increases, the absorption will gradually increase and the reflected signal will gradually decrease. From this curve, it can be seen that by calculating the test frequency of the signal, the depth information of the signal can be inverted based on its linear relationship, that is, the defect depth information can be obtained. According to the spacing relationship be-

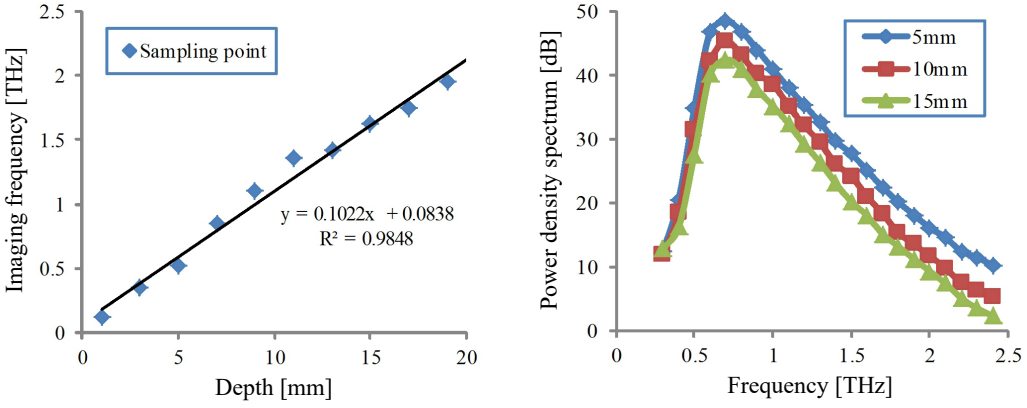

Fig. 6. Parameter relationship for quantitative identification of defects. (a) Curve of imaging frequency and depth. (b) Curve of frequency and power spectral density.

tween the test points in the figure, the depth accuracy of the defect is about 2.5 mm. As shown in Fig. 6(b), when the frequency is below 0.5 THz, the defect and the frequency domain signal of the reference signal are basically the same. When the frequency increases between 0.55 and 2.4 THz, the overall power spectral density shows a trend of first increasing and then decreasing, and gradually decreases with the increase of defect depth. Throughout the entire testing frequency, the relationship between the frequency domain signal power spectral density and frequency for defects at three different depths is also essentially the same.

6. Conclusions

The paper investigates a THz time-domain detection system for internal defects in CFRP plates and proposes a defect analysis algorithm based on multi-layer gradient threshold to calculate defect parameters. The THz time-domain spectra of CFRP plates were obtained experimentally, and the reconstruction of two-dimensional THz images of CFRP plates was completed using a multi-layer gradient thresholding algorithm. The experimental results show that there is a good linearity between defect depth and testing frequency. The size of the defect area can be calculated through THz time-domain imaging. The depth information of defects has good consistency with THz power spectral density.

The paper realizes the measurement of the size and depth of different types of defects in CFRP plates, and achieves accurate measurement of different echo response intensities through multi-layer gradient threshold algorithm. The goal of quickly identifying debonding defects and crack defects has been achieved. The average relative error of defect size recognition can reach 3.63%, and the linearity of depth recognition can reach 0.98. It verifies the feasibility of the system, which can be applied to non-destructive testing of CFRP sheet materials in various fields.

Acknowledgment

This work was supported by Shanxi Province Higher Education Science and Technology Innovation Project (2023L357) and Shanxi Province Teaching Reform and Innovation Project (J20241891) and The Ministry of Education collaborates with industry and academia to promote collaborative education (241103177012203).

References

[1] NASLAIN R., *Design, preparation and properties of non-oxide CMCs for application in engines and nuclear reactors: An overview*, Composites Science and Technology **64**(2), 2004: 155-170. https://doi.org/10.1016/S0266-3538(03)00230-6

[2] SCHELLER M., KOCH M., *Fast and accurate thickness determination of unknown materials using terahertz time-domain spectroscopy*, Journal of Infrared, Millimeter, and Terahertz Waves **30**, 2009: 762-769. https://doi.org/10.1007/s10762-009-9494-6

[3] HALABE U.B., VASUDEVAN A., KLINKHACHORN P., GANGARAO H.V.S., *Detection of subsurface defects in fiber reinforced polymer composite bridge decks using digital infrared thermography*, Nondestructive Testing and Evaluation **22**(2-3), 2007: 155-175. https://doi.org/10.1080/10589750701448381

[4] KAWASE K., SHIBUYA T., HAYASHI S., SUIZU K., *THz imaging techniques for nondestructive inspections*, Comptes Rendus Physique **11**(7-8), 2010: 510-518.
[5] ZANDONELLA C., *T-ray specs*, Nature **424**, 2003: 721-722. https://doi.org/10.1038/424721a
[6] ZHAO H., WANG G., MA T., *Based on THz spectroscopy detection method for the concentration of 1,3-dinitrobenzene volatile gas*, Guang Pu Xue Yu Guang Pu Fen Xi (Spectroscopy and Spectral Analysis) **32**(4), 2012: 902-905. [Article in Chinese]
[7] WANG G., XU D., YAO J., *Research on detecting explosive content of 2,4-dimitroanisole based on THz spectroscopy*, Guang Pu Xue Yu Guang Pu Fen Xi (Spectroscopy and Spectral Analysis) **33**(4), 2013: 886-889. [Article in Chinese]
[8] DESTIC F., BOUVET C., *Impact damages detection on composite materials by THz imaging*, Case Studies in Nondestructive Testing and Evaluation **6**, 2016: 53-62. https://doi.org/10.1016/j.csndt.2016.09.003
[9] REN J.J., LI L.J., ZHANG D.D., QIAO X.L., LV Q.Y., CAO G.H., *Study on intelligent recognition detection technology of debond defects for ceramic matrix composites based on terahertz time domain spectroscopy*, Applied Optics **55**(26), 2016: 7204-7211. https://doi.org/10.1364/AO.55.007204
[10] WANG H.N., REN J.J., ZHANG D.D., GU J.A., ZHANG J.Y., LI L.J., *Glass fiber reinforced polymer terahertz feature enhancement and defect imaging based on continuous wavelet transform*, Acta Materiae Compositae Sinica **38**(12), 2021: 4190-4197.
[11] ZHANG J.Y., REN J.J., LI L.J., GU J., ZHANG D.D., *THz imaging technique for nondestructive analysis of debonding defects in ceramic matrix composites based on multiple echoes and feature fusion*, Optics Express **28**(14), 2020: 19901-19915. https://doi.org/10.1364/OE.394177
[12] LIN J., QI J., ZHANG Y.Q., ZHANG W., CHEN Y., HE M.X., QU Q.H., ZHANG Y.Z., *Layer classification algorithm in terahertz thickness measurement technology*, Chinese Journal of Lasers **51**(18), 2024: 1801017 [Article in Chinese]. https://doi.org/10.3788/CJL240955
[13] XU Z., XU D.G., LIU L.H., LI J.N., ZHANG J.X., WANG T., REN X., QIAO X.M., JIANG C., *Metal microstrip line defect detection of chip based on THz-TDR technology*, Journal of Infrared, Millimeter, and Terahertz Waves **43**(3), 2024: 361-370 [Article in Chinese]. https://doi.org/10.11972/j.issn.1001-9014.2024.03.010
[14] COSTIL S., LUKAT S., BERTRAND P., LANGLADE C., CODDET C., *Surface treatment effects on ceramic matrix composites: Case of a thermal sprayed alumina coating on SiC composites*, Surface and Coatings Technology **205**(4), 2010: 1047-1054. https://doi.org/10.1016/j.surfcoat.2010.07.021
[15] FEDERICI J.F., WAMPLE R.L., RODRIGUEZ D., MUKHERJEE S., *Application of terahertz Gouy phase shift from curved surfaces for estimation of crop yield*, Applied Optics **48**(7), 2009: 1382-1388. https://doi.org/10.1364/AO.48.001382
[16] LOPATO P., CHADY T., *Terahertz detection and identification of defects in layered polymer composites and composite coatings*, Nondestructive Testing and Evaluation **28**(1), 2013: 28-43. https://doi.org/10.1080/10589759.2012.694882

Received March 4, 2025
in revised form March 29, 2025